Slope stability assessment of an open pit mine using 3 dimensional rock mass modelling

Morales M.[1]; Panthi K. K.[2], Botsialas K.[3]

[1,2]Norwegian University of Science and Technology (NTNU), Trondheim, Norway

[3] The mining company, AS.

Abstract

Rock mass classification systems are commonly used to evaluate the likelihood of instability in mining environments. Most frequently used classification systems are RMR, GSI, and Q-system. These methods are used widespread among geotechnical engineers as one practical way to assess quality of the rock mass. In most of hard rock open pit mines, bench faces with no clear discontinuities present one or two joint sets that may dominate on the failure mechanism. To address this, Slope Mass Rating (SMR), which is a modified version of RMR system of rock mass classification, can be used. The benefit is that SMR takes into consideration the influence of joint orientation on the classification method itself. Hence, the main aim of this paper is: first, to develop a 3-dimensional RMR model of an open pit mine under active operation based on the extensive field mapping carried out, and then produce a SMR surface model that is derived using current topography, modeled RMR values and jointing conditions prevailing in each structural domain. The final goal is to create a SMR susceptibility map of the mine area for the dominant topographic condition and the main structural domains present in the open pit, and to present a methodology that may be easily replicated at any given hard rock open pit mine. The authors emphasize that the use of SMR model is a very helpful tool in evaluating the areas of the mine that are most vulnerable to potential slope instability in different periods of operation of the mine.

Keywords: Slope stability, rock mechanics, rock mass model, mining slope, mining geotechnics.

1.   Introduction

Open pit mining excavates the earth surface in order to reach the underlying valuable ore. Planning of an open pit is a matter of determining the most profitable pit limit and the most economical mining sequence for a given mineralization (Steffen et al, 1970). During exploitation phase, the excavation sequence implies the development of artificial slopes on which stability is a crucial factor both for safety and financial viability of the mining. Therefore, the stability assessment of an open pit rock slope is an essential requirement of the open pit mine not only during the feasibility and detail design studies but also throughout the operational life of the project. Rock mass classification systems are extensively and often used to quantitatively classify the quality of the exposed rock mass in the open pit slopes. There are varieties of rock mass classification systems that have been proposed in the last 50 years. Four of these classification systems have gained broad acceptance in the mining industry, which are the Rock Mass Rating (RMR) of Bieniawski (1973), the Norwegian Q-system (Barton et al, 1974), the MRMR (also known as

Laubscher's RMR) updated by Laubscher (1990), and the GSI system proposed by Hoek (1994) and later modified by Marinos and Hoek (2000). Flores and Karzulovic (2002) described that the most used method of rock mass classification in underground mines is MRMR, which accounts 53%, followed Q-system (26%) and RMR system (15%). On the other hand, the most used method of rock mass classification in open pit mining is Hoek's GSI (39%), followed by RMR (26%) and MRMR (22%). The disadvantages and limitations of rock mass classification systems with respect to stability assessment of slopes have been discussed in detail by Pantelidis (2009).

In addition to the above mentioned methods of rock mass classification systems the Slope Mass Rating (SMR), which is an adjusted version of RMR and was proposed by Romana (1985), has gained acceptance in recent years, especially for pit slope and cut slope stability assessments. According to Aksoy (2008) the direct application of RMR for slopes may in some occasion give meaningless results. The SMR is a rock mass rating tool for risk based evaluation of slope instability at a particular slope face and its relation with discontinuities prevailing in the rock mass. The SMR adjusts RMR-values by accounting four more factors as explained by Equation 1 (Romana, 1985).

$$SMR = RMR - (F1 \cdot F2 \cdot F3) + F4 \qquad (1)$$

The product of three factors (F1, F2 and F3) is an adjustment rating directly related to the discontinuity systems prevailing in the rock slope. The first factor (F1) accounts for the parallelism of the strikes of the discontinuities and the slope face, the second factor (F2) for the dipping angle of the discontinuities, the third factor (F3) for the relation between the slope face angle and the dip of the discontinuity, and the last factor (F4) accounts for the influence by the quality blasting (or excavation method) into the slope face. Tomás et al (2007) proposed an alternative way then was originally proposed by Romana (1985, 1993) to calculate first three factors of SMR based on the continuous functions. The authors demonstrated that these functions show maximum absolute difference with discrete functions lower than 7 points.

Many authors have applied geostatistics to investigate fracture distribution in the rock mass (Long, 1987; Chiles, 1988; Rafiee, 2008) and to estimate different rock mass properties (Yu, 1993; Ellefmo, 2009). Similarly, the interpolation of areas of same RMR level based on point observations in the field has been proposed as a suitable method to extend the point ratings to a surface by Öztûrk (2002) and Ryu (2003). Ferrari (2014) revealed that the resulting RMR map based from spatial estimation by geostatistical analysis can be a useful tool to estimate the quality of outcropping rock mass and to assess the geotechnical behavior of the mapped area. RMR rating index is being assessed using geostatistical analysis since early 2000, especially for underground projects. The kriging method is being extensively used to both borehole and surface datasets. RMR values have always been considered as a single regionalized variable (Stavropoulou, 2007 and Exadaktylos, 2008b), and also as the sum of many variables (Egaña an Ortiz, 2013). The Q-system is being estimated as a single variable by geostatistical methods analyzing its effects on the Tunnel Boring Machine related parameters (Exadaktylos, 2008a). However, one should note that there are limitations in each classification system as discussed by Palmstrom and Broch (2006) and Marinos (2005). If carefully used, these classification systems can provide very useful information on slope stability during planning and design stage as well as during construction and operation phases. In addition, classification systems can also be used to assess the properties of the rock mass in a very systematic and standardized way (Hoek, 2006).

This manuscript tries first to interlink and compare the rock mass quality class assigned using three different classification systems (RMR, Q and GSI) aiming to develop a 3-dimensional rock mass model of an open pit mine located in Norway based on RMR system of rock mass classification. The manuscript further assesses possible unstable areas in the open pit mine slope by adjusting the RMR values to SMR values combining the mine topography with detailed information of slope orientation, slope angle and main jointing orientations achieved

from the 3D-structural model developed by Morales et al (2017). Development of such SMR surface model is helpful to reveal large-scale and bench scale potential movements in the pit slope, which are critical components for risk management practices in slope stability similar as discussed by Panthi and Nilsen (2006). Due to sensitivity no detailed information of the ore body, including location of the mine, will be provided in the manuscript, which has no implication on the research outcome of this manuscript.

2.   Brief about open pit mine case

The open pit mine has been in operation over 60 years now and is a major hard-rock deposit of its kind known today. The geometry of the slope is defined by a first pass to define an initial single bench height of 15 meters, which is doubled in the second pass to have an overall height of 30 meters. Therefore, overall slope angle of the mine is between 45 to 55 degrees. The open pit has a length of approximately 3 km and the current depth is close to 240 meters from the top. The mining activity is planned to continue for many year to come and will extend the depth of the pit significantly from what it is at present. Therefore, short, medium and long term stability is a crucial issue for this mine.

2.1.   Geology

The area is characterized by a great anorthosite intrusion in which the ore body is intruded. The structure of the ore becomes increasingly complex in the east. Xenoliths of anorthosite are present within the ore body. The anorthosite, which is located within the ore body or in the contact zones of the ore body typically shows more alteration than in the surrounding rock mass of the pit slope. Two major diabase dikes crosscut the ore body at WNW-ESE direction. These dikes have straight appearance and dip almost vertical. The largest main dike (furthest to the south) is about 25 meters wide (Figure 1). As main dike exits the ore body in the east, it forms swarm of several smaller dikes extending from the main body. Several studies have shown that there are some areas of heavy alteration that are related to fractures and fault systems at the mine site, on both ore body and anorthosite.

Structural domains

Morales et al (2017) have shown that there are six different regional lineaments, which are correlated with the regional pattern of discontinuities. In this manner it was also possible to distinguish six different fracture systems (FS) in the mine area. Based on the jointing associated to each of these fracture systems, a total of 8 structural domains were identified and 3D structural model was presented. Structural domains are in general not concretely defined (Read and Stacey, 2009) with a fixed boundary between them, but rather created in such a way that overlapping is possible to better interpret the transition between structural domains.

These structural domains are associated to one or more fracture systems; as for example the case of structural domain 08, which is associated to FS6 in the upper portion of the hanging wall in the northwestern part of the mine. The structural domains are possible to be seen in Figure 1, while Table 1 summarizes the structural domains and major joint sets associated to different fracture systems (FS).
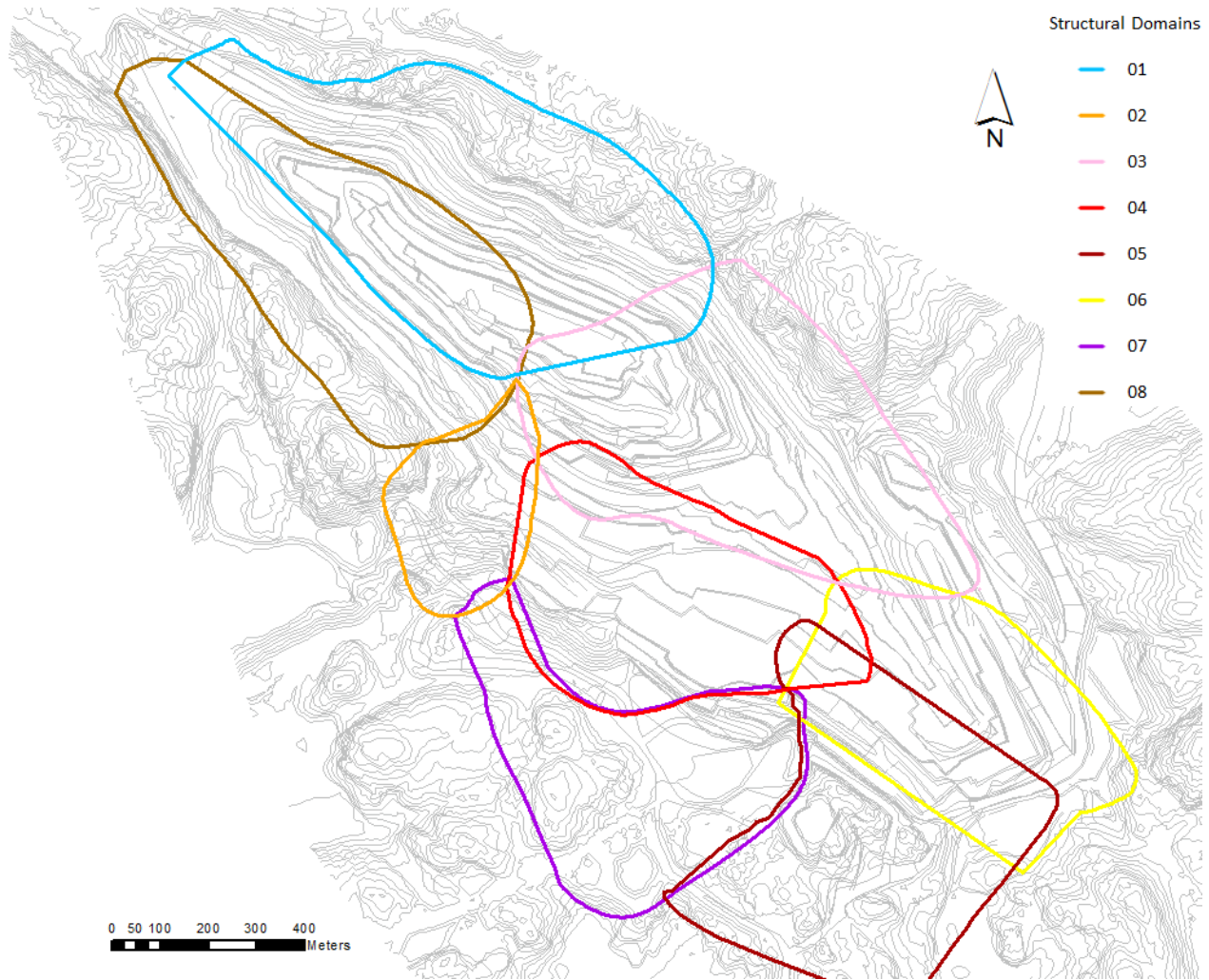
Figure 1: Map of the mine area with structural domains (modified from Morales et al, 2017).

Table 1: Structural domains with jointing direction and associated fracture systems in the mine area (modified from Morales et al, 2017).

Structural Domain	Joint Set			Associated FS		
	J1	J2	J3	to J1	to J2	to J3
01	89/029	89/268	-	FS5	FS1	-
02	77/269	63/346	-	FS1	FS3	-
03	84/314	78/218	76/025	FS2	FS5	FS4
04	43/051	56/356	75/219	FS6	FS3	FS5
05	85/040	-	-	FS4	-	-
06	78/272	81/239	82/216	FS1	FS5	FS4
07	84/128	-	-	FS2	-	-
08	49/054	-	-	FS6	-	-

3.   Methodology

The development of the Rock Mass Model is based in two sources of information; i.e. the surface mapping of the mine that assigns RMR, Q and GSI values to the mapped zone and the underground mapping, which is achieved through the inspection and analysis of boreholes and mapping of drainage tunnels. The surface mapping provides a bi-dimensional interpretation of the distribution of the quality, which at some extent is close to be tridimensional since the mapping is done in m-benches at different z-coordinates. On the other hand, the borehole offers information in a specific point along the axis that could be extrapolated to two or three dimensions when combined with other boreholes in the neighborhood. Therefore, these two layers are combined in order to build the most possible accurate 3-dimensional interpretation of the quality of the rock mass in the mine area.

The method begins with data acquisition, in which field mapping is done in selected positions along the open pit, inside the drainage tunnels and core logging. Collected individual parameters are associated to estimate RMR and Q values. In addition, GSI values were estimated based on the visual inspection of the slope. After the data has been collected, validation was carried out and comparison between RMR and GSI against Q was made in order to verify if the rock mass ratings assigned to each one are in line with the typical relationships proposed by Bieniawski (1989) and Hoek (1997). This may not indicate whether the rating is well assigned since rock mass classifications are highly subjective and relative to the one involved in the mapping. However, it is for certain that it will provide a sound basis for evaluating equal criteria when assessing different methods. These first two steps are the ones necessary to create a sound database for further work.

Once the database has been generated, preliminary surfaces maps for RMR, GSI and Q distribution were interpolated into GIS software. The parameters were set to RMR values and calculated accordingly to GSI and Q. For validation of these parameters the database is split into two subsets: modelling and control. Further, 80% of the data are kept on the part of modelling subset, while remaining 20% were kept for quality control. The ratio of 80% and 20% was successfully used by Egaña an Ortiz (2013) in the validation of RMR values. This procedure is repeated 5 times with 5 randomly generated datasets following the 80/20 rule in order to quantify the error. The result of this stage is the preliminary contours and isocurves based in certain threshold values were extracted from the map. Each threshold was selected based on the typical quality class range. The contours were also smoothed in order to avoid peaks or strange geometries in the final output.

In parallel, an assessment of RMR values in boreholes was done. As the purpose of the research is to produce a SMR model, the quality assessment of the rock mass from boreholes was carried out using RMR. Low RMR zones were identified and correlated with the structural model of the mine developed by Morales et al (2017). The structures that influenced in lowering down RMR values in the boreholes and estimated by field mapping were added to the preliminary contours. Finally, surface contours of RMR values were developed by considering discontinuity structures affecting the quality of the rock mass and were added to the ArcGIS model.

Further, based on the RMR data from boreholes, a preliminary 3-dimensional RMR model was developed. The outcome of this step does not necessarily have to match the final surface contouring of the RMR values. Hence, the 3-dimensional model was later adjusted with the surface information from the final contours and incorporated into the model to match the RMR values mapped at the surface. The output was the final 3-dimensional distribution of RMR describing 3D rock mass quality model.

After the creation of 3D rock mass quality model based on RMR, SMR values were calculated in the pit surface taking in account the finalized RMR values, the dip and the dip direction from the slope face and the jointing information. The information on jointing was traced from the already established structural domains of the mine by

Morales et al (2017). The SMR map was developed for both the total slope and for the slope in bench scale. This is necessary to assess scale effect on the potential instability condition of the pit slope for short-term, medium-term and long-term and also to verify correctness of our assessment with the areas potentially prone to instabilities. A diagram illustrating how steps are performed in order to create the model is presented in Figure 2.
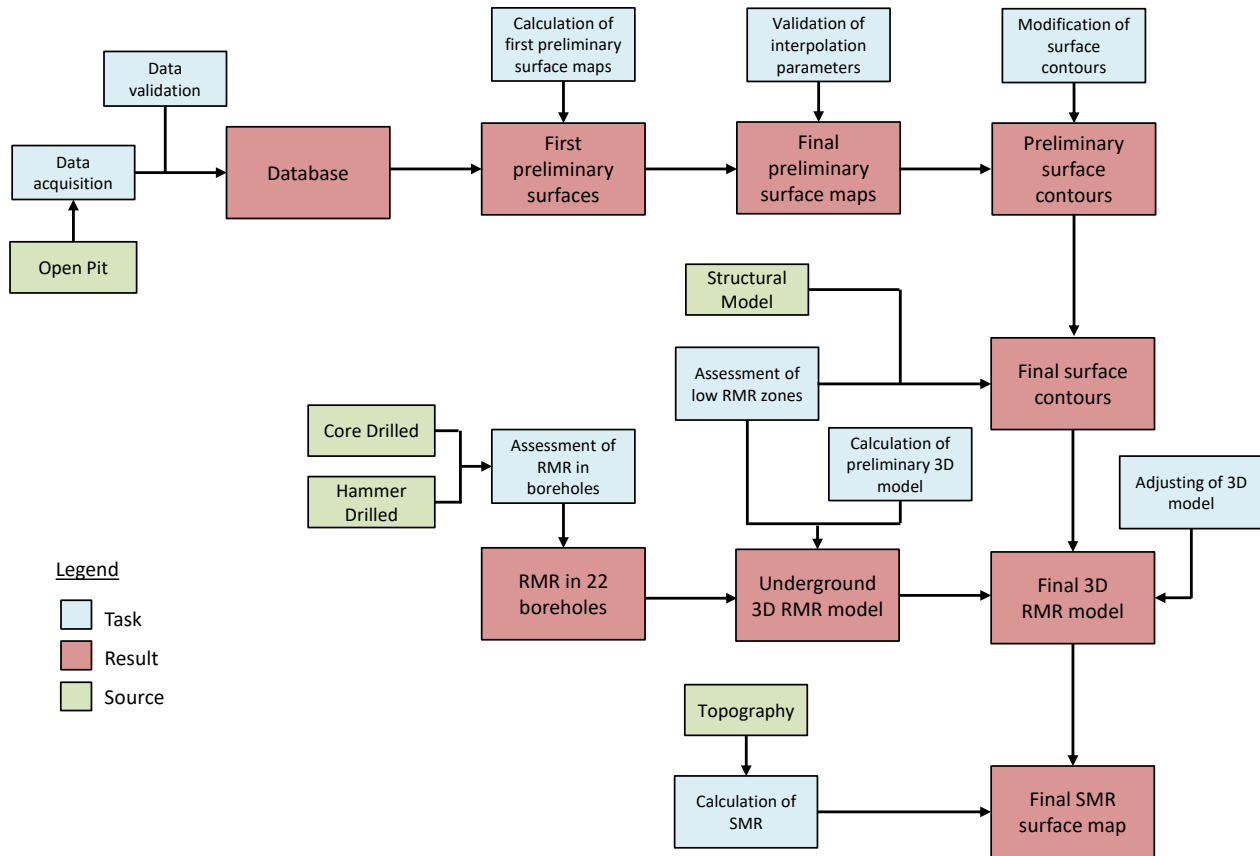

Figure 2: Flowchart for the calculation of surface SMR maps based on topography and 3-dimensional RMR distribution.

4. Field work and data acquisition

Data gathering and correct interpretation is extremely important since quality of accumulated date sources are mainly responsible for the quality of the end model. Some of the important steps of data accusation were as following:

- Study on regional geology, regional faulting, main lineaments and placement of the ore body is very important and has close relationship with the different lithological and structural domains in the mine pit.

- Structural mapping of the different domains and rock types control both bench design and overall stability. This includes both joint sets as well as major features such as dykes, faults, contacts, etc.

- Identification of alteration zones within the pit is important. Alteration affects rock strength; therefore, different alterations within the same rock type were grouped separately.

- Laboratory testing of different rock types with the results grouped by alteration for each rock type.

4.1. Surface Mapping

The surface mapping was done in the summer months of years 2015 and 2016. It consisted mainly in performing the following 5 steps in every location:

1. Measuring orientation (dip/dip direction) for each joint set that was possible to access.
2. Schmidt hammer testing of the most unfavorable exposed joint surface.
3. Assessment of RMR parameters.
4. Assessment of Q parameters.
5. Estimation of GSI value.

The mapping covered most of the mine area that was accessible during the field work period. A total of 197 surface points were logged. The distribution of the mapping locations is shown in the Figure 3. The figure also shows the location of drill holes (core drill and hammer drill holes).
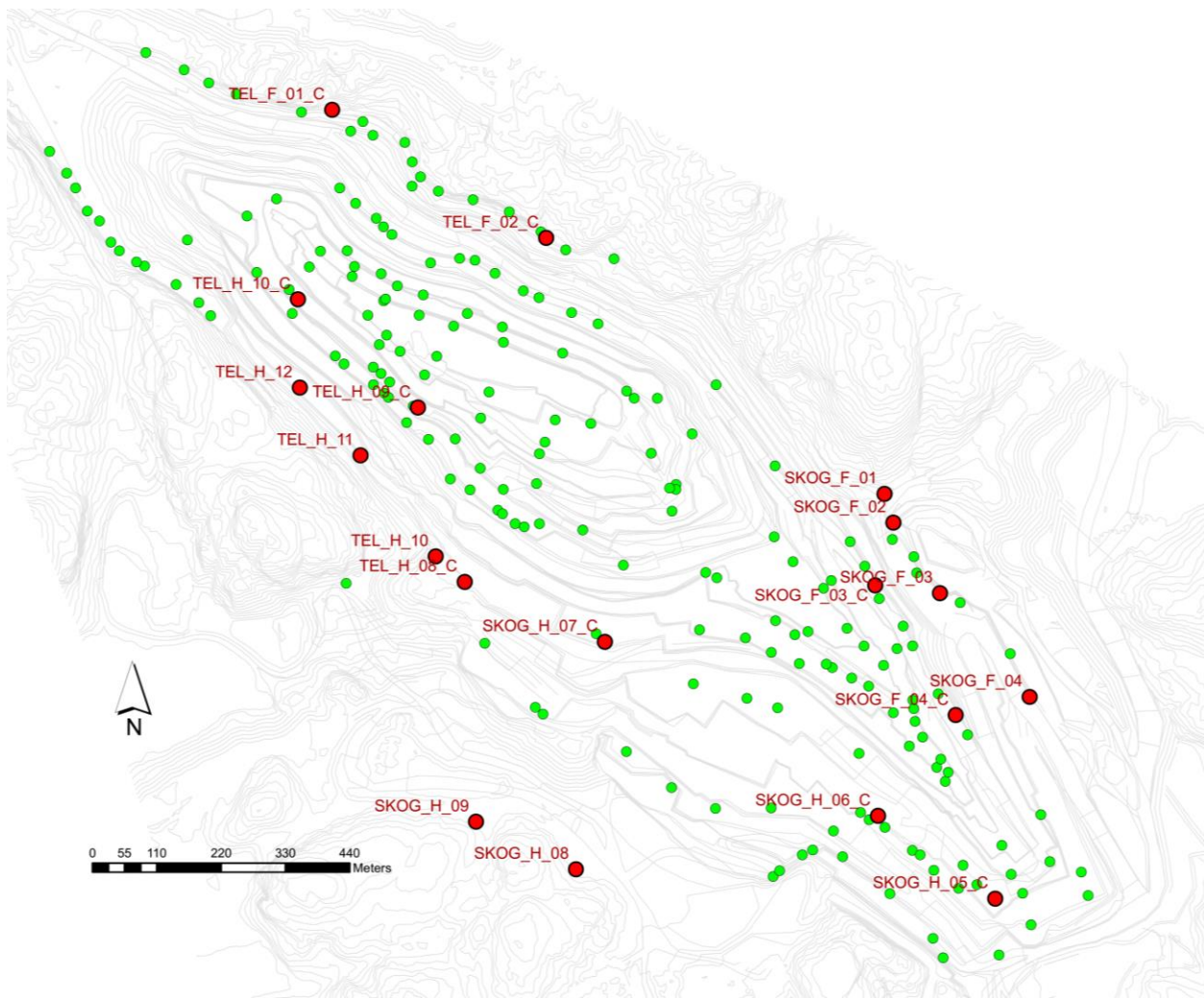

Figure 3: Distribution of surface mapping locations (green dots) along the mine.

In order to assess the reliability of the rating assigned in the field, RMR, GSI, and Q ratings were compared. In this aspect, it is well known from Bieniawski (1989) and Hoek (1997) that there are two relationships between RMR and Q and GSI:

$$RMR = 9 \cdot ln\,(Q) + 44 \qquad (2)$$

$$RMR = GSI + 5 \qquad (3)$$

Combining (2) and (3) gives:

$$GSI = 9 \cdot ln\,(Q) + 49 \qquad (4)$$

The measurements for RMR and GSI were plotted against the Q value in order to stablish if they follow (or not) the relationships given above. The resulting graph (Figure 4) shows that the best fit for each dataset are approximately as following:

$$RMR = 8 \cdot ln\,(Q) + 53 \qquad (5)$$

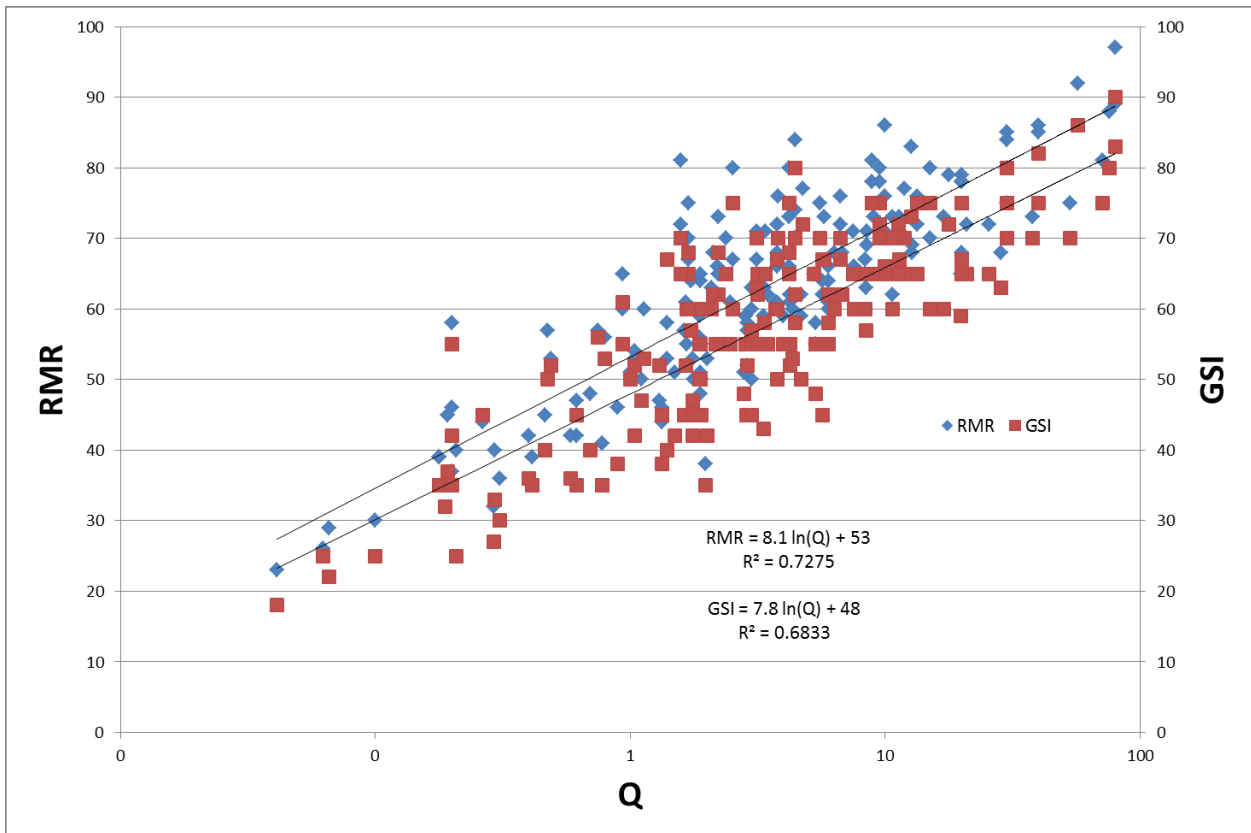$$GSI = 8 \cdot ln\,(Q) + 48 \qquad (6)$$

Figure 4: Comparison of RMR and GSI ratings against Q-value.

By combining Equation 5 and 6 will give exactly similar results as expressed by Equation 3 suggesting that the correlation achieved through the mapping results are valid to interpolate from one rock mass classification to the other, which increased the reliability level of the classification achieved through field mapping.

4.2.   Underground Mapping

The idea of interpreting a RMR rating based on information from Boreholes is not a straightforward process, since it needs a lot of assumptions and generalizations in order to assign correct and prudent values. The project has a total of 22 boreholes (Figure 3). 10 of them are core drilled, which were manually logged in 2015 and 2016. The remaining 12 holes are hammer drilled, and the available information was through geophysical logging. Different assumptions were made for each of the two sets of boreholes, since the information coming from both is not equal.

4.2.1.   Core drilled boreholes

Core drilled boreholes were logged every 1m core length registering RQD, total core recovery (TCR), solid core recovery (SCR), frequency of fractures per meter (FFm), number of joint sets, weathering index, and strength index. Also for each open fracture, the roughness index (JRC), alteration number (Ja) and approximated basic friction angle, and the weathering of filling material were recorded. Closed fractures were also registered in position. In order to calculate the RMR, the parameters were derived based on as following:

1. Uniaxial compressive strength: the rating was assigned from the UCS obtained for samples coming from the different lithology in the area, and tested in the laboratory. Each segment of the borehole length has an associated lithology.
2. Rock quality designation (RQD): direct from the core logging.
3. Spacing of discontinuities. Based on the total number of joint sets and FFm. If there are no joints, then it was assumed to be more than 1m.
4. Condition of discontinuities
   a) Length, persistence: not possible to obtain directly. It was assigned a common value based on 15m persistence, since it is the height of benches in the mine.
   b) Aperture: direct from the core logging.
   c) Smoothness: JRC directly measured in the core logging and it was transformed into RMR rating following Table 2.
   d) Infilling: derived from the alteration number Ja, assessed directly from the core.
   e) Alteration / weathering: assessed directly from the exposed open joint walls.
5. Groundwater conditions: not possible to obtain, the rating has been assumed as wet.

Table 2: RMR rating assigned to roughness profile (JRC as in Barton & Chubey 1977).

JRC	RMR rating
0-2	0
2-4	0
4-6	1
6-8	1
8-10	3
10-12	3
12-14	5
14-16	5
16-18	6
18-20	6

4.2.2. Hammer drilled boreholes

Hammer drilled boreholes were logged recording data every 5cm through geophysical inspection with acoustic televiewer (Riglar, 2014). The method is able to register the position of a joint and calculate its aperture, dip and dip direction. Other parameters associated, like estimated content of potassium, are also possible to derive from the results. To calculate the RMR, the ratings were evaluated as following:

1. Uniaxial compressive strength: Same as for the core drilled boreholes.
2. Rock quality designation (RQD): Calculated from the number of fractures given for a length of 1m.
3. Spacing of discontinuities. Calculated from the position of each fracture. If there are no joints, then it was assumed to be more than 1m.
4. Condition of discontinuities
   f) Length, persistence: not possible to obtain directly. It was assigned a common value based in 15m persistence, same as to the core drilled boreholes.
   g) Aperture: direct from the core logging.
   h) Smoothness: A surface mapping campaign for recording values of dip, dip direction, JRC, and amplitude (in a 10cm, 20cm and 1m scale) was carried out in the summer of 2016. The values were then analyzed to find a correlation between the roughness rating assigned via RMR and the Dip/Dip Direction. The results of the investigation are shown in Table 3. JRC values were transformed into rating following the ratings shown in Table 2.

Table 3: Average roughness rating and JRC class per fracture system.

Fracture System	Amplitude profile rating [cm]			Avg rating	Avg JRC	RMR rating
	10	20	100			
FS1	6.00	5.50	5.00	5.50	16-20	5
FS2	1.41	2.06	2.88	2.12	6-10	2
FS3	5.75	5.50	6.00	5.75	18-20	6
FS4	3.22	3.49	2.65	3.12	8-12	3
FS5	3.92	4.25	3.64	3.94	10-14	4
FS6	3.40	3.55	2.50	3.15	8-12	3

   i) Infilling: it was calculated from the potassium and thorium content. Geophysical logging was performed inside the hammer drilled boreholes. Part of the logging was the Spectral Gamma Sonde, which measures the different energy level respecting to the different radioactive elements. The calculated curves of K-40, Uranium and Thorium concentrations were assessed and the anomalies of potassium and thorium against depth, were used in order to define presence of clayey minerals
   j) Alteration / weathering: it was derived from the potassium and thorium content, since there is a correlation to the presence of alteration zones.
5. Groundwater conditions: Flowmeter tests along with hydraulic tests, like slug tests, double and single packer tests, were used in order to derive the fractures that are water bearing. The RMR rating was based on the results of these tests and the estimation of flow. It has been assumed to a rating of 7 for the rest of the boreholes without flow testing, assuming a moderately wet condition.

5. Development of the model

5.1. Preliminary maps and surface validation

RMR, Q and GSI surface maps were developed based on the results from the field mapping. Among diverse kriging methods, You and Lee (2006) and Choi (2009) have used indicator kriging to estimate RMR classes. Since the RMR values of the study area fall within only three classes, the ordinary numerical kriging was selected as was done by Ferrari (2014) and Stavropoulou (2008) instead of indicator kriging. It is highlighted here that the indicator kriging needs an indicator transformation, which all the time needs extra information about significantly high or significantly low values falling within the same class. However, whether a value is slightly big or very big than the chosen threshold in fact does not play a significant role. Therefore, ordinary kriging was chosen to take in account the entire data set range. An ordinary Kriging gives the best linear unbiased prediction of the intermediate values between two field measurement points. The method uses 3 parameters to the estimation, which were analyzed and established as following:

- **Major range:** Represents a distance beyond which there is little or no correlation. Trials were done with 50, 100, 200 and 400m. The maps represented by 50 and 100m are not characteristic enough (contradicting with the field experience) of what it is possible to understand in the mine. There is also small difference between 200m and 400m, and the last one was used as definitive number. Ferrari (2014) noted that in 2D models the minimum mean error has been obtained by performing kriging on the longest lag distance, and he used 1000m as the range in a regional scale. Hence, it should be understood that the chosen range (400m) represents fairly good extent considering local scale for this mine.

- **Partial sill:** The difference between the nugget and the sill. A value of 80 was used after trying 50, 70, 80 and 95. It is logical to accept this value as representative since the highest possible RMR that was mapped in the mine was around 85.

- **Nugget:** Represents the error and variation at spatial scales too fine to detect. The nugget effect is seen as a discontinuity at the origin. Trials were done with 5, 10 and 20, being 5 the value selected.

In every resulting surface map, contours were developed according to rock mass class. The division of the isolines was made following the criteria proposed by Panthi (2006), which is presented in Table 4. As seen in the table, GSI was also added based in equation (3).

Table 4: Rock mass classes used for classification (modified from Panthi, 2006)

	Descriptions	Range of Q-values		Range of RMR-values		Range of GSI-values	
Rock Class	Quality	Min	Max	Min	Max	Min	Max
1	Very good to excellent	100	1000	85	100	90	100
2	Good	10	100	65	85	70	90
3	Fair to good	4	10	56	65	61	70
4	Poor	1	4	44	56	49	61
5	Very poor	0.1	1	35	44	40	49
6	Extremely poor	0.01	0.1	20	35	25	40
7	Exceptionally poor	0.001	0.01	5	20	10	25

In order to test the final values, a validation of the model was carried out by splitting the RMR database into two subsets; i.e. the first 80% of the data were used as the modelling subset and the remaining 20% were used as control set for the validation purpose as was successfully used by Egaña an Ortiz (2013) in validating RMR values. This procedure was repeated 5 times with 5 randomly generated datasets following the 80/20 rule in order to quantify the error. This repetition is necessary to try to isolate errors associated to the occurrence of lower values (i.e. less than 40) as much as possible since values below 40 are not very common and hence may lead to a biased interpretation of the results. Evaluating the control points against the interpolated value gave an average error of 16% compared to the expected value. Since the error is relative to the RMR value in a certain position, the expected variation was considered relatively less for low RMR values than for high RMR values. Egaña and Ortiz (2013) reported errors from 7% to 11% in a direct estimation of RMR. Therefore, the parameters used and achieved surfaces were considered as within acceptable limit. Using relationships between RMR and GSI as well as RMR and Q represented by Equations (2) and (3), the parameters were defined following the same criteria for the interpolation of GSI and Q surface maps. The interpolated final maps with 100% data are shown in Figure 5.
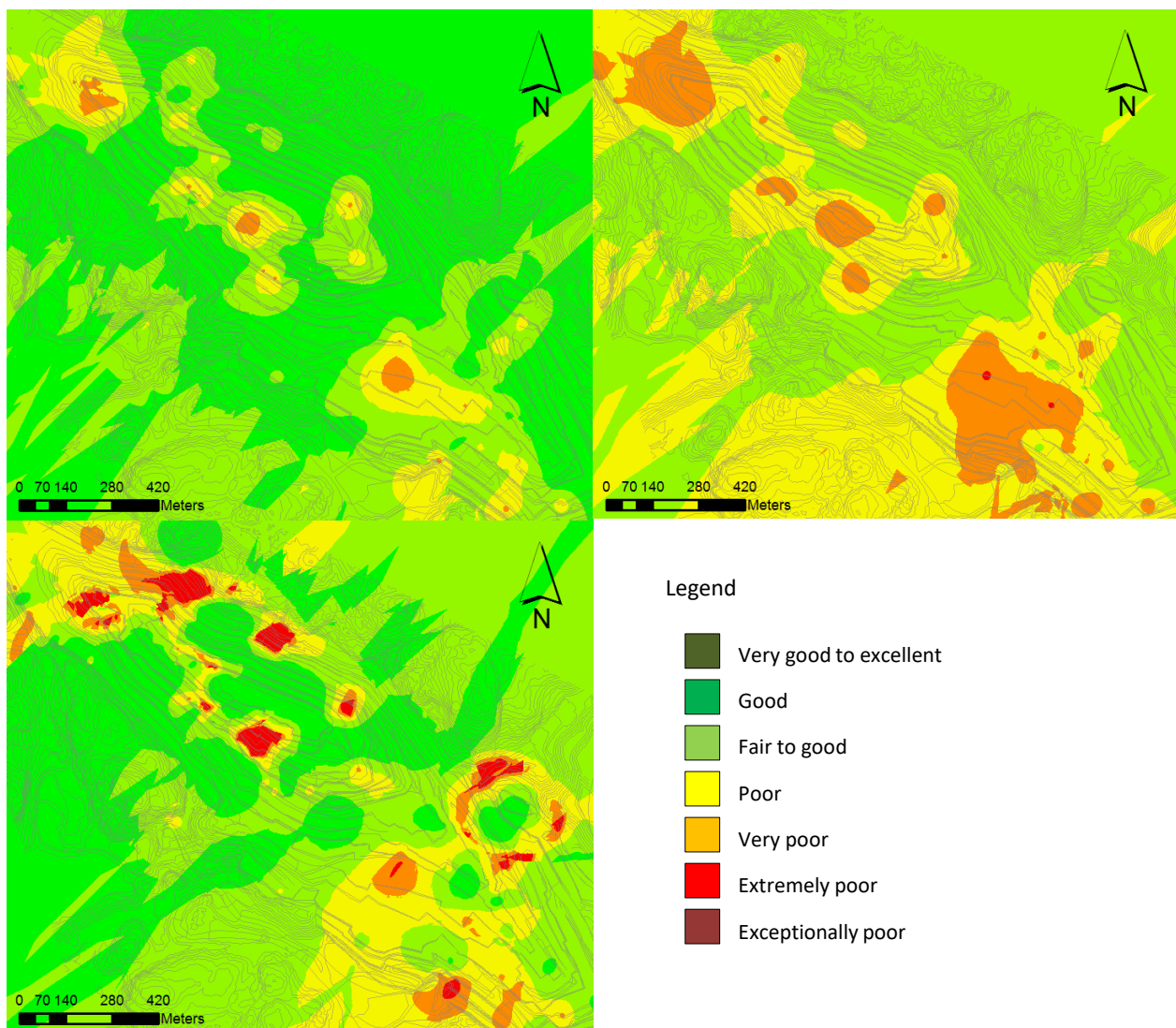

Figure 5: Surface interpolation of RMR (up left), GSI (up right) and Q (down left).

5.2. RMR contours from surface mapping

The resulting contours were modified taking in account the spatial distribution of the field measuring points so that the surface outside the main area of measurements were assigned as "more constant" values. As no measurements were made in the south western part of the mine that can support the idea of a certain value in that part of the map, contours were smoothed considering better interpretation of what was possible to see in the field. This also applies to the north east part of the mine. It was interpreted that contours are only rational to be defined only along the mine, and were adjusted to the most typical value outside (were no data is available). A comparison between the original contours and the smoothed and corrected contours is presented in Figure 6.
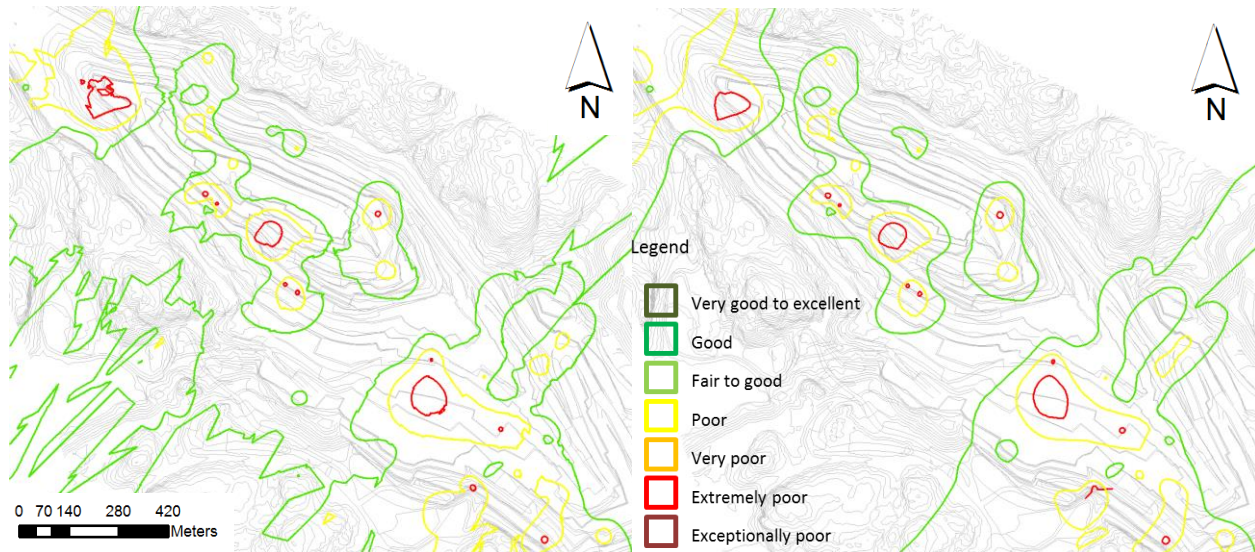

Figure 6: Contours for RMR distribution; left - directly extracted from kriging and right - smoothed and modified according to actual field conditions.

5.3. Correlation between surface maps and borehole RMR

After the surface RMR map was defined, in the next step it was tried to correlate between the mapped values at the surface of the mine and mapped values based on information from the borehole loggings. Low RMR zones were identified in each borehole according to the same criteria presented in Table 4. After identifying low RMR zones in each borehole, efforts were placed to analyze RMR values for each interval considering dip and dip direction of the dominant discontinuities. Rigler (2016) has shown that there is a good agreement of the fractures per meter recorded via geophysical and manual logging of the boreholes. Highly fractured zones are very likely to be accurately recorded at the same depth from both methods of logging. Low RMR zones identified through borehole logging were correlated against the major discontinuity planes mapped in the surface. If consistent agreement between the mapped results from borehole logging and surface mapping were found then the whole plane was assumed to have influenced on the low RMR zone and the contour was modified accordingly. A total of 19 planes were identified to have an agreement, which were intersecting the boreholes at a certain depth. Table 5 shows the interval and the predominant dip and dip direction of the discontinuities compared to surface mapped discontinuities presented in the structural model (Morales et al, 2017).

Table 5: Low RMR zones found in boreholes correlated to big planes from structural mapping of mine surface.

Borehole	From borehole log					From surface mapping		
	RMR	From	To	Dip	DipDir	RMR	Dip	DipDir
SKOG_F_03_C		70.4	75.4	83	116		76	126
SKOG_H_06_C		80.5	84.5	63	270		70	290
TEL_F_01_C		43.6	48.5	76	262		65	232
TEL_F_01_C		43.6	48.5	72	120		70	118
SKOG_F_04_C		14.1	50.1	78	230		75	215
SKOG_F_04_C		14.1	50.1	70	64		62	44
SKOG_E_05		63.0	70.0	61	46		75	50
SKOG_F_01		27.0	37.0	83	336		63	352
SKOG_F_01		118.0	119.0	50	184		52	178
SKOG_F_02		7.0	20.0	82	126		76	126
SKOG_F_02		62.0	63.0	77	132		76	126
SKOG_F_02		106.0	118.0	81	297		88	278
SKOG_F_03		71.0	86.0	86	144		90	327
SKOG_F_04		34.0	49.0	78	221		70	230
SKOG_H_09		219.0	224.0	72	322		71	338
TEL_H_08_C		36.4	42.1	63	336		64	345
TEL_H_10		22.0	24.0	48	56		47	57
TEL_H_11		52.0	53.0	65	162		40	142
TEL_H_12		182.0	184.0	75	269		70	270

The low RMR zones were then incorporated into the surface contours with defined new low RMR zones associated to surface mapping planes shown in Table 5. Modified contours are presented in Figure 7, which is also the final and modified version of RMR surface map.
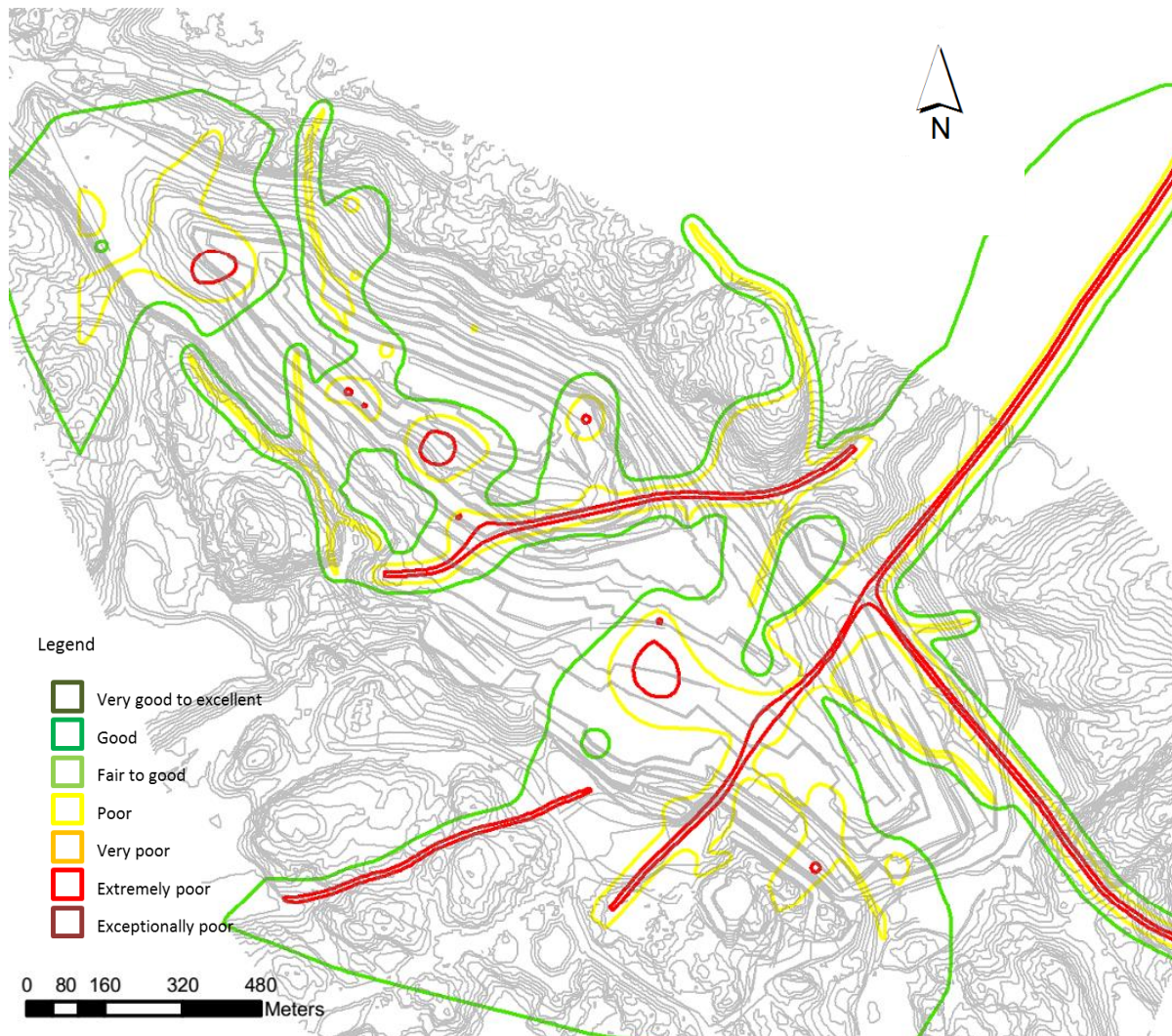
Figure 7: Finally adjusted contours for RMR distribution in the open pit.

5.4.   3-dimensional RMR model

Exploiting information presented above a 3-dimensional RMR model was developed in Leapfrog Geo software. The main objective of the modelling was to be able to establish a correlation between what it was possible to derive from the boreholes information (underground) and the open pit surface mapping. The development of 3-dimensional distribution of RMR was an important milestone for the project, since it will help to estimate rock mass quality rating in future geometries of the open pit, which will also work as the baseline information for the calculation of SMR.

The process started with the interpolation of volume enclosing the different rock mass quality class presented in Table 4. Only 5 quality classes (class 2 to class 6) were relevant for this open pit since no rock mass classes with category 1 and 7 were registered during mapping. The 3D-modelling continued with the process of "surface outcrop fitting", which involved the modelling of each zone associated to every plane with low RMR zones. In this way, it was possible to assign the corresponding dip and dip direction to each plane allowing surface areas to extend as volumes into the rock mass aiming to intersect previously identified weakness zones. Figure 8 shows the

general fitting of the final rock mass quality contours at the pit topography including isometric and cross section view. Section A-A' gives possibility to recognize a plane that defines a low-RMR zone just behind the mine slope (and also daylighting at some benches). This joint set is comparable with the field observation of a joint system called crusher system (FS6) in the hanging wall
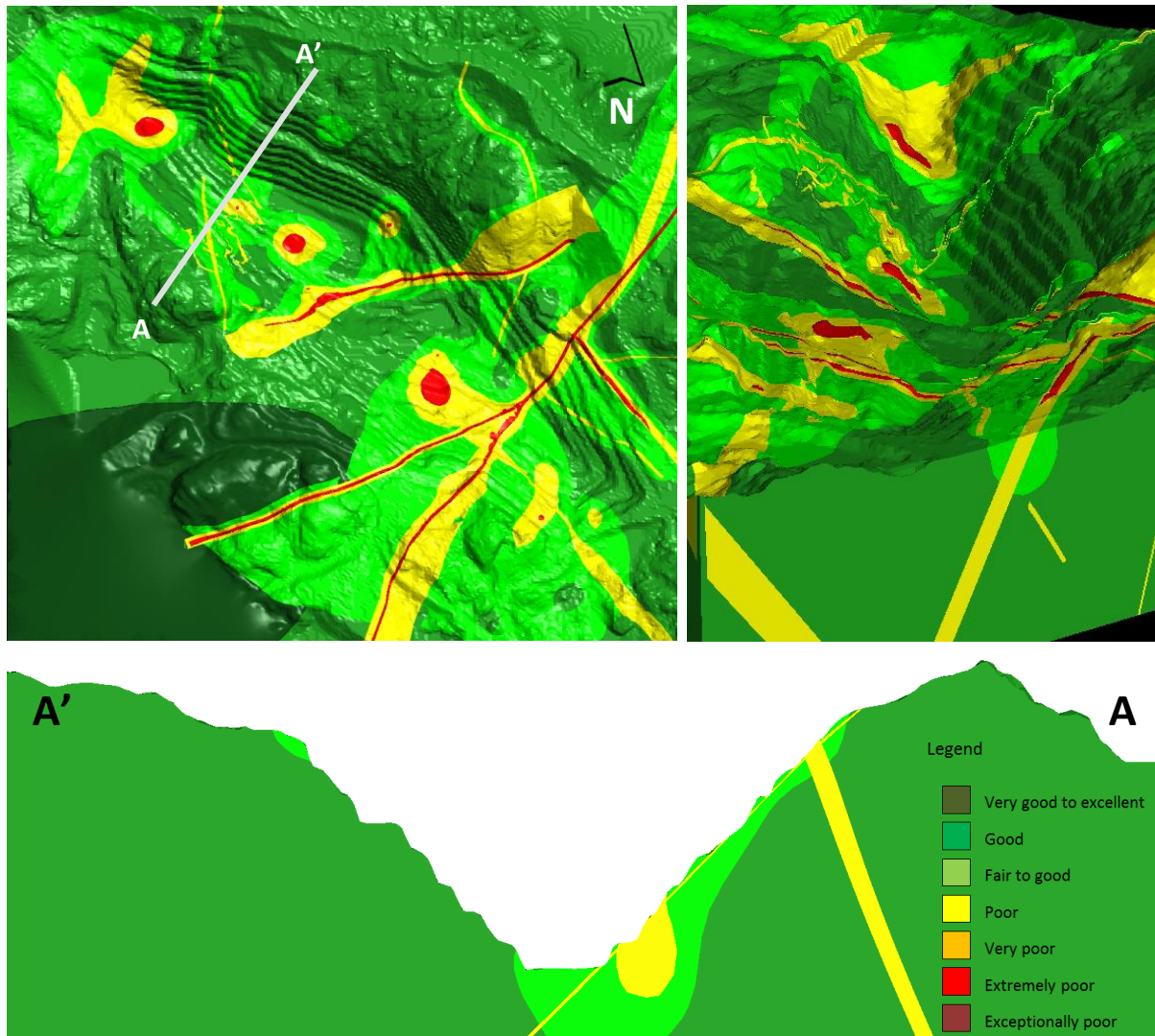

Figure 8: Final 3-dimensional RMR distribution. Plan view (up left), isometric from the south east (up right), and section A-A' (down).

From the RMR-map it is clear that the areas that may be prone to instabilities are located in the hanging wall (HW). The north eastern part is associated to the occurrence of joint planes related FS6 in structural domain 08 whereas the south west part is more associated to bench scale events. The developed RMR map was correlated and verified at the field and showed good level of agreement. Morales et al (2017) also identified and discussed possible failure geometries in both bench and slope scale of the mine for each structural domain. The results indicates that the possibilities for slope scale failure geometries and bench scale failure geometries are mainly present in the hanging wall (HW), while small block falls and toppling may be possible to happen throughout the entire pit. This can also be seen through the low values of RMR in the model.

It is also possible to derive from the 3D-RMR model that most of the low ratings RMR zones are distributed along the hanging wall of the pit, especially in the upper benches of the north-western part and in the south-eastern portion. This distribution is in accordance with the behavior of the mine that has been observed in the field, as well as from registered instability events at the pit in the past.

5.5.   The SMR model

The calculation of the SMR was done in ArcMap following equations proposed by Tomas (2007), also known as the Continuous Slope Mass Rating (CSMR). The CSMR was computed using an equation, which is similar to discrete SMR, but the difference lies in calculating the adjustment factors (F1, F2 and F3) depending on the joint-slope relationship. The functions showed maximum absolute difference with discrete functions lower than 7 points and significantly reduced subjective interpretations. Similarly, the functions for SMR correction factors reduce doubts about what score to assign to values near the border of the discrete classification. On the other hand, the factor F4 is same for both SMR and CSMR. The functions are defined as following:

$$F_1 = \frac{16}{25} - \frac{3}{500} arctan\left(\frac{1}{10}(|A| - 17)\right) \qquad (7)$$

Where A = $\alpha_j - \alpha_s$ difference of dip directions of joint and slope for planar failure.

$\alpha_i - \alpha_s$ difference of dip directions of line of intersection and slope for wedge.

$\alpha_j - \alpha_s - 180$ difference of dip directions of joint and slope plus 180 for toppling.

$$F_2 = \frac{9}{16} + \frac{1}{195} arctan\left(\frac{17}{100}B - 5\right) \qquad (8)$$

Where, B is equal to the dip (β_j) of joint for planar failure and toppling, and to the dip of line of intersection for wedge failure.

$$F_3 = -30 + \frac{1}{3} arctan(C) \qquad (9)$$

$$F_3 = -13 - \frac{1}{7} arctan(C - 120) \qquad (10)$$

Where C = $\beta_j - \beta_s$ difference of dips of joint and slope for planar failure, in Eq 9.

$\beta_i - \beta_s$ difference of dips of line of intersection and slope for wedge, in Eq 9.

$\beta_j + \beta_s$ sum of dip of joint and slope for toppling, in Eq 10.

The stability classes and qualitative description proposed by Romana (1985) are also applicable to the CMSR values (table 6).

Table 6: Stability classes according to SMR values (Romana, 1985).

Class	I	II	III	IV	V
SMR	81-100	61-80	41-60	21-40	0-20
Rock mass description	Very good	Good	Normal	Bad	Very bad
Stability	Completely stable	Stable	Partially stable	Unstable	Completely unstable
Failures	None	Some block failure	Planar along some joints or many wedge failure	Planar or big wedge failure	Big planar or soil-like or circular

In order to effectively calculate the SMR, 5 different layers of information were needed. Those layers were combined pixel to pixel for the calculation of final SMR map. The necessary layers comprise; 1) dip of the slope, 2) dip direction of the slope, 3) RMR values, 4) distribution of adjustment factor for excavation method (F_4), and 5) the structural domains that contains the information about dip and dip direction of the major joint sets. The slope layer was considered in 2 different ways: one layer with the overall slope angle, and other layer with the bench face angle. Also inside each structural domain and based on the kinematic analysis presented by Morales et al (2017) joint sets leading to planar, wedge or toppling failure were considered. The joint sets were accounted for an average dip and dip direction. The standard deviation of the dip and the dip direction of each joint set were considered in order to reflect the most likely directions of each joint set to assess the worst case condition.

Following this process two resulting maps for each joint set in each structural domain were developed consisting; 1) SMR map for the entire slope of the mine and 2) SMR map for the bench scale of the mine. If the purpose was to have just one final map, these maps might be later combined with a minimum function, in order to preserve the smaller value on each pixel. However, the authors do not recommend merging the maps since there exists the risk that SMR map may loss its meaning due to the different scale of the problem (bench versus slope). Finally the SMR map for each structural domain was combined to produce the final SMR map of the pit. This was accomplished by merging of the raster keeping the minimum value where overlaps were present. As seen in Figure 1, the structural domains are overlapped. The overlapping allows to achieve better interpretation of reality, since transitions between structural domains are not strictly defined, but are most commonly seen as areas were joint sets of different structural domains coexists. A diagram illustrating the SMR calculation process is shown in Figure 9.
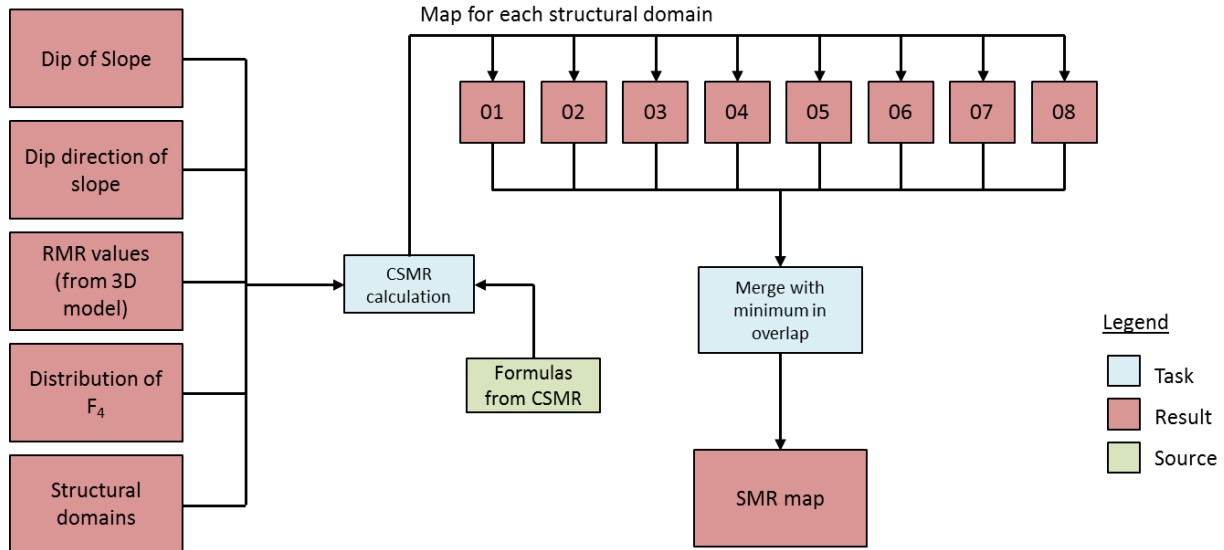
Figure 9: Detailed flowchart followed for the SMR calculation.

A total of 16 local maps (for each of the 8 structural domains for both bench and slope scale) were produced and finally combined in order to produce two final SMR maps as shown in Figure 10.
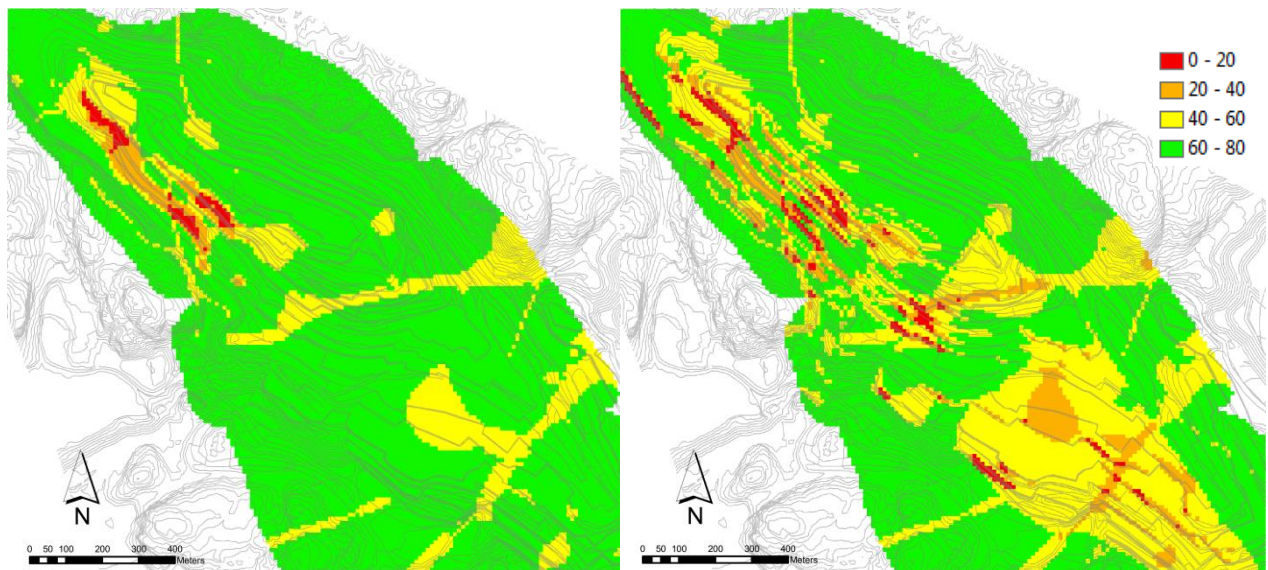

Figure 10: Final SMR map for the total slope (left) and for the bench slope (right).

From the maps it is clear to note that the possible areas that may be prone to instabilities are located in the hanging wall (HW) in both total and bench scales. The north eastern part is associated to the occurrence of persisting fracture system (FS6) in structural domain 08, which may lead to instabilities both in bench and slope scale. On the other hand, the south western part is most likely associated to bench scale events, as no distinct low SMR areas exist at the slope scale. It is emphasized here that as the mining operation at present is mainly focused in the south western part of the pit, the overall slope angle is less than 35 degrees and the topography is relatively flat at this stage of the mining.

Morales et al (2017) identified the failure geometries at both bench and slope scale for each structural domain. The authors concluded that both slope scale and bench scale failure geometries are possible in the hanging wall of the mine, while small block falls and toppling may happen throughout the pit. In this regards the structural domains 02, 04 and 08 are the ones that possess slope scale as well as bench scale instabilities. This behavior is also possible to be distinguished in Figure 11, where SMR map is combined with structural domains of the mine.
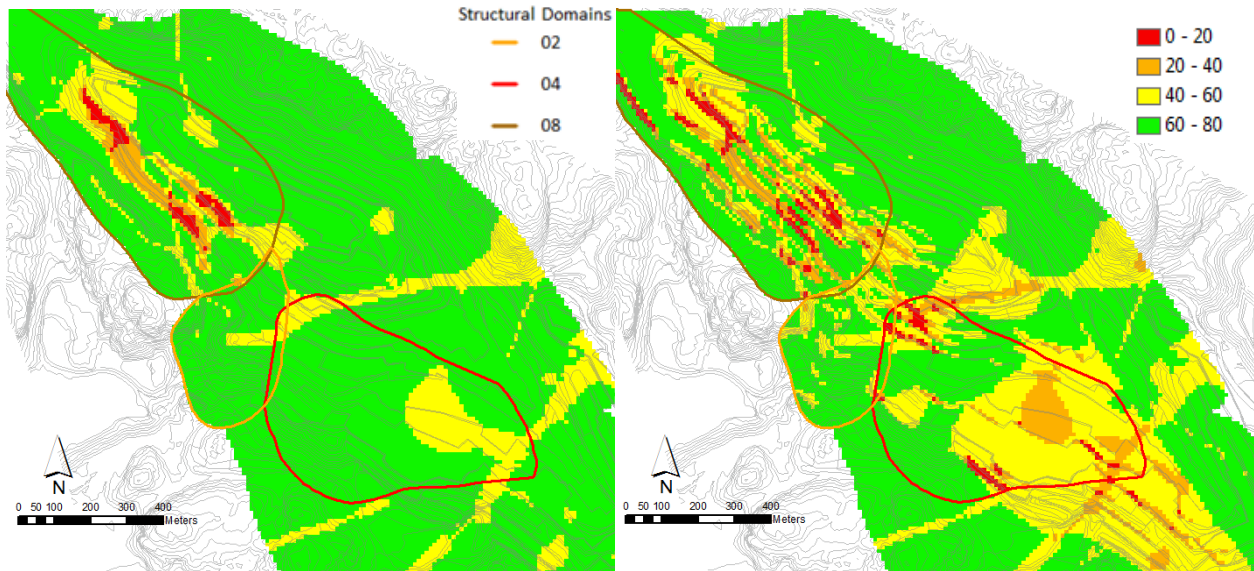

Figure 11: Final SMR map with structural domains for total slope (left) and for bench slope (right).

6.   Discussion

In general terms one can conclude that the bench scale map is being able to depict the stability conditions in a good level of agreement with what is possible to perceive in the field. There are small inaccuracies coming from the fact that structural domains are more generalizations of average conditions within certain limits. As is possible to recognize, the imprecisions are found on the boundaries of the structural domains. As identified in the field, there are 3 zones showing lower quality than presented above, which occur mainly in the border of structural domain 08 approaching to structural domains 01 and 02. These inaccuracies are highlighted in Figure 12.

On the other hand, the overall slope map is not as accurate as expected. In the south eastern area it fails to depict the current conditions, while in the north western part of the pit, it gives slightly coarse image of the areas prone to instabilities (Figure 12). There are two reasons that explain this result:

1. When the structural domains were defined, the amount of fractures mapped on the surface was much bigger than those that were taken in account from the boreholes. As a result, the 3D envelopes of the domains are more accurate close to the slope face and not that much when going deeper, while the influence of the information from boreholes becoming dominating. So, if we had "220 boreholes" and not only 22, then the reliability would have been much higher. The percentage of mapped joints on the surface corresponds to 77% meaning only 23% of the information was coming from the mapping of boreholes.

2. The overall slope angle is a reinterpretation of the current topography based in the creation of new contours from a surface generated from the topography. As the distance and baseline for the new

contours are decided arbitrarily, the value of SMR might be slightly different if one selects different parameters in order to create the base map.
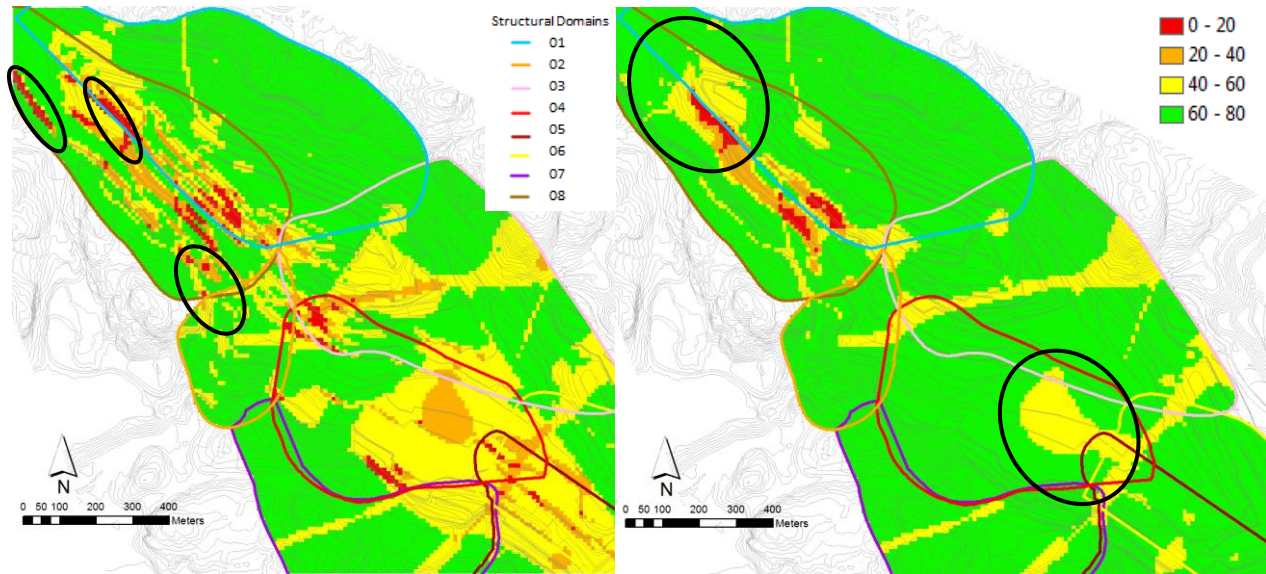

Figure 12: Zones with underestimated SMR quality in total slope (left) and bench slope (right).

Therefore, the SMR maps presented here should give somewhat conservative interpretation of the conditions of the slope around the mine as highlighted by Romana (2001). Similarly, it is equally important to mention here that none of the zones (both total slope and bench slope) that are currently facing unstable conditions were avoided by this analysis, i.e. the value of the SMR index has not been overestimated.

7. Conclusions

The comparative study in correlating links between different rock mass classification method has indicated fairly good agreement as suggested by Bieniawski (1989) and Hoek (1997), which gave possibility further develop a 3-dimensional rock mass model of the mine. The development of 3D rock mass model of the pit gave an overview of RMR values in space, which is useful to identify areas with low RMR ratings all along the hanging wall of the pit. This distribution is in agreement with the behavior of the mine that has been observed in the field, as well as from past recorded instability events. However, it is important to note that there are areas where RMR surface maps with low ratings are not always linked to potential failure modes. It is also well known that in hard rock open pit mining, the failure modes are defined by slope geometry and orientation and their character of the discontinuities prevailing at both the total slope and the bench scale slopes. The SMR map showed that most likely slope scale instabilities will be concentrated in the hanging wall, while bench scale failures may potentially appear in both hanging wall and in foot wall at the southeastern area of the mine. As demonstrated here, the SMR map provides much enhanced picture of the stability situation of the open pit than that of the 3D-RMR model. In addition, it is highlighted here that the stability assessment based on only geometrical analysis with for example a joint set dipping at 82 degrees and having direction parallel to the bench face dipping at 85 degrees fulfills the criteria of a plane failure may necessarily not mean that the slope will fail since the failure will depend on the frictional properties of the most vulnerable discontinuity set in question.

This research has also demonstrated that calculating a SMR surface values from a 3 dimensional RMR model is very fruitful methodology not only for assessing present events, but also it helps to assess potential future instability events since this can be easily seen by developing future topographic condition of the mine for short, medium and long-term mine plan. Moreover, the 3D- RMR model may be used to predict rock mass conditions by intersecting the domains with future pit topographies, and later to calculate the SMR in order to depict future stability conditions. The presented methodology can be replicated in any other open pit mine with a similar level of geotechnical information. Hence, the development of 3D-picture of the rock mass should be incorporated as a part of the mine plan so that all short, medium and long-term challenges are visualized and appropriate measures are in place to avoid serious and significant future instabilities.

References

Aksoy, C.O. (2008) *Review of rock mass rating classification: Historical developments, applications, and restrictions.* Journal of Mining Science 44(1), pp 51-63.

Barton N.R., Lien R., Lunde J. (1974) *Engineering classification of rock masses for the design of tunnel support*. Rock Mech vol6(4), pp 189–239.

Bieniawski, Z.T. (1973) *Engineering classification of jointed rock masses*. Trans South African Institute of Civil Engineering vol15, pp 335–344.

Bieniawski, Z.T. (1989) Engineering *rock mass classifications. A complete manual for engineers and geologists in mining, civil, and petroleum engineering.* John Wiley and Sons, Inc, 251p.

Chilès, J.P (1988). *Fractal and geostatistical method for modelling a fracture network*. Math Geol;20(6) pp. 631–654

Choi, Y., Yoon, SY., Park, HD. (2009). *Tunneling analyst: a 3D GIS extension for rock mass classification and fault zone analysis in tunneling*. Comput Geosci, vol 35, pp 1322–33.

Egaña, M., Ortiz, J. (2013) *Assessment of rmr and its uncertainty by using geostatistical simulation in a mining project.* Journal of GeoEngineering, vol 8, no.3, pp. 83-90.

Exadaktylos, G., Stavropoulou, M., Xiroudakis, G., de Broissia, M., Schwarz, H. (2008a) *A spatial estimation model for continuous rock mass characterization from the specific energy of a TBM*. Rock Mech Rock Eng;41, pp 797–834.

Exadaktylos, G., Stavropoulou, M. (2008b) *A specific upscaling theory of rock mass parameters exhibiting spatial variability: analytical relations and computational scheme.* Int Journal Rock Mech Min Sci;45, pp 1102–25.

Ellefmo, S.L., Eidsvik, J. (2009) *Local and spatial joint frequency uncertainty and its application to rock mass characterisation*. Rock Mech Rock Eng ;42 (4), pp. 667–688.

Ferrari, F., Apuani, T., Giani, G.P. (2014) *Rock Mass Rating spatial estimation by geostatistical analysis.* International Journal of Rock Mechanics & Mining Sciences 70, pp 162–176.

Flores, G., Karzulovic, A. (2002) *Geotechnical guidelines for a transition from open pit to underground mining.* Benchmark report. Project ICS-II, task 4.

Hoek, E. (1994) *Strength of rock and rock masses*. News J ISRM 2(2):4–16.

Hoek, E. (1997) *Practical estimates of rock mass strength*. International Journal of Rock Mechanics and Mining Sciences, Vol 34, No 8, 1997, pp 1165-1186.

Hoek, E. (2006) *Practical Rock Engineering.* e-notes available at Hoek's corner. www.rocscience.com

Laubscher, D.H. (1990) A Geomechanics classification system for the rating of rock mass in mine design, J.S Afr. Inst. Mining Metallurgy, vol. 90, no 86, pp. 257- 273.

Long, J.C.S, Billaux, DM. (1987). *From field data to fracture network modelling: an example incorporating spatial structure*. Water Resour Res;23(7). pp, 1201–1216.

Marinos, P., Hoek, E. (2000) *GSI: a geologically friendly tool for rock mass strength estimation*. In: Proceedings of the GeoEng2000 at the international conference on geotechnical and geological engineering, Melbourne, Technomic publishers, Lancaster, pp 1422–1446

Marinos, V., Marinos, P., Hoek, E. (2005) *The geological strength index: applications and limitations.* Bull Eng Geol Environ (2005) 64, pp 55–65.

Morales, M., Panthi, K.K., Botsialas, K., Holmøy, K.H. (2017) *Development of a 3D structural model of a mine by consolidating different data sources*. Bulletin of Engineering Geology and the Environment. Accepted and in the process of publication.

Öztürk, C.A. (2002). *Geostatistical assessment of rock zones for tunneling*. Tunneling and Underground Space Technology 17, pp 275–285

Palmstrom, A., Broch, E. (2006) *Use and misuse of rock mass classification systems with particular reference to the Q-system*. Tunnels and Underground Space Technology, 21, 575-593.

Pantelidis, L. (2009). *Rock slope stability assessment through rock mass classification systems*. International Journal Rock Mech Min Sci 46(2), pp 315–325

Panthi K.K., Nilsen B. (2006) Numerical analysis of stresses and displacements for the Tafjord slide, Norway. Bull Eng Geol Env, vol. 65, pp 57–63.

Panthi K.K. (2006) *Analysis of engineering geological uncertainties related to tunneling in Himalayan rock mass conditions*. Doctoral thesis, Norwegian University of Science and Technology, ISBN 82-471-7826-5.

Read, J., Stacey, P. (2009). Guidelines for Open Pit Slope Design. ISBN: 9780643094697, pp 69-82.

Rafiee, A., Vinches, M (2008). *Application of geostatistical characteristics of rock mass fracture system in 3D model generation*. International Journal Rock Mech Min Sci;45: pp. 644–652.

Riglar, B., Botsialas, K., Morales, M. (2016). Structural characterization of hard rock formation using wireline borehole logging techniques in an open pit mine, Norway. Proceedings of the 17th Nordic Geotechnical Meeting, NGM Reykjavik 2016, pp 1203-1212.

Romana, M. (1985) *New Adjustment Ratings for Application of Bieniawski Classification to Slopes*, Proceedings of International Symposium on the Role of Rock Mechanics, ISRM, Salzburg, pp. 49-53.

Romana, M. (1993) *A geomechanical classification for slopes: slope mass rating*. Comprehensive rock engineering, John A. Hudson, Editor-in-Chief, pp 575–600.

Romana, M., Serón, J.B., Montalnar, E. (2001). La clasificación geomecánica SMR: aplicación experiencias y validación. In proceedings of V Simposio Nacional sobre Talues y Laderas inestables. Madrid, pp.393-404.

Ryu, D.W, Kim, T.K, Heo, J.S. (2003). *A study on geostatistical simulation technique for the uncertainty modeling of RMR*. Tunnel and Underground 13:87–99

Stavropoulou, M., Exadaktylos, G., Saratsis G. (2007) *A combined three-dimensional geological-geostatistical-numerical model of underground excavations in rock*. Rock Mech Rock Eng;40(3), pp 213–43.

Steffen, O.K.H., W. Holt, V. R. Symons. (1970) *Optimizing Open Pit Geometry and Operational Procedure*. In Planning Open Pit Mines, Proc Symposium on the Theoretical Background to the Planning of Open Pit Mines with Special Reference to Slope Stability. Johannesburg, August 29- September 4, 1970, pp. 9-31.

Tomás, R., Delgado, J. & Serón, J.B. (2007) *Modification of slope mass rating (SMR) by continuous functions*. International Journal of Rock Mechanics and Mining Sciences 44, pp 1062-1069.

You, K., Lee, JS. (2006) *Estimation of rock mass classes using the 3-dimensional multiple indicator kriging technique*. Tunn Undergr Space Technol; 21 (3-4):229.

Yu, Y.F., Mostyn, G.R. (1993). *Spatial correlation of rock joints*. Probabilistic methods in geotechnical engineering. Rotterdam: Balkema.

COVER LETTER

The manuscript is a continuation of our manuscript titled "Development of a 3D structural model of a mine by consolidating different data sources" which is under publication at the Bulletin (BOEG-D-16-00756R1).

Authors came in conclusion that this manuscript is also submitted to this journal to achieve coherence in the way that the reader finds it easy to interlink both manuscripts.

The authors are confident that the Bulletin of Engineering Geology and the Environment will have the same opinion about the reviewed version incorporating both the comments from the editor and reviewer.